

# Calculation and analysis of complex band structure in dispersive and dissipative two-dimensional photonic crystals.

Y. Brûlé and G. Demésy

*CNRS, Aix-Marseille Université, Centrale Marseille,  
Institut Fresnel UMR 7249, 13013 Marseille, France*

B. Gralak

*CNRS, Aix-Marseille Université, Centrale Marseille,  
Institut Fresnel UMR 7249, 13013 Marseille, France and  
Corresponding author: boris.gralak@fresnel.fr*

(Dated: September 21, 2018)

Numerical calculation of modes in dispersive and absorptive systems is performed using the finite element method. The dispersion is tackled in the frame of an extension of Maxwell's equations where auxiliary fields are added to the electromagnetic field. This method is applied to multi-domain cavities and photonic crystals including Drude and Drude-Lorentz metals. Numerical results are compared to analytical solutions for simple cavities and to previous results of the literature for photonic crystals, showing excellent agreement. The advantages of the developed method lie on the versatility of the finite element method regarding geometries, and in sparing the use of tedious complex poles research algorithm. Hence the complex spectrum of resonances of non-hermitian operators and dissipative systems, like two-dimensional photonic crystal made of absorbing Drude metal, can be investigated in detail. The method is used to reveal unexpected features of their complex band structures.

## I. INTRODUCTION

Spectral or modal analysis is an essential tool to deal with resonance phenomena in optics – or wave physics in general – since it provides the natural excitation conditions of the system. In optics, metallic structures are of particular interest, since they support a vast variety of resonances, resulting from plasmon and geometric structuration. These resonances are defined as the eigenfrequencies and corresponding eigenmodes associated with the spectral problem of source free Maxwell's equations.

Metallic structures are classically described by frequency dependent permittivity given by Drude or Drude-Lorentz models [1]. In this situation the operator involved in the spectral problem of Maxwell's equations depends on the frequency as well as the material dispersion relation. The spectral problem becomes non linear, and generally non-hermitian when dissipation takes place. Hence the eigenfrequencies lie in the complex plane and the computation of the whole spectrum of resonances is a challenging task.

Numerical calculation of the complex resonances has been performed for two dimensional photonic crystals in the cases of square [2] and circular [3] rods. These pioneering calculations have been performed using numerical codes solving time-harmonic Maxwell's equations combined with a *poles search* algorithm in the complex plane, making the tool difficult to use in practice. Hence, new techniques have been proposed and used to determine the complex resonances. For instance, as for photonic crystals, generalizations of the well-known plane wave expansion method have been implemented [4, 5]. In the case of monotonic dispersion relation, *e.g.* away from the materials intrinsic resonances, the cutting plane

method as proven to be an effective numerical work-around [6, 7]. Finally, finite difference schemes based on the Yee grid have been proposed in [8] or [9]. In this last reference, the technique is based on the introduction of additional fields leading to an extended system where the frequency dispersion is eliminated, which represents a decisive advantage for numerical calculations. This framework appears to be a derivation of the auxiliary field formalism introduced by A. Tip [10, 11] in order to consider rigorously Maxwell's equations with frequency dispersion and absorption. Indeed, in this formalism, auxiliary fields are added to the electromagnetic field to express Maxwell's equations with an hermitian operator independent of time. Thus, the auxiliary field formalism [10, 11] is the general frame leading to the rigorous treatment of absorption and to significant simplification of frequency dispersion.

In this article, a version of the auxiliary field formalism is established in order to allow the linearization of the spectral problem associated with frequency dispersive materials described by Drude or Drude-Lorentz model. A variational form of the resulting augmented system is derived and is then implemented into the Finite Element Method (FEM). Next, the presented method is compared to semi-analytical results for two dimensional multi-domain closed cavities. Finally, the method is successfully applied to two-dimensional photonic crystals made of Drude materials and the fully exhibited richness of the obtained complex spectrum of resonances is discussed.

## II. THE SPECTRAL PROBLEM

### A. Setup of the problem

Let  $\mathbf{x}$ ,  $\mathbf{y}$  and  $\mathbf{z}$  be the unit vectors of the orthogonal Cartesian coordinate system  $O_{xyz}$  and  $(x, y, z)$  the coordinates of the vector  $\mathbf{r}$ . The time-harmonic regime is considered with a  $\exp(-i\omega t)$  time dependence, where  $\omega$  is the possibly complex valued frequency. The electromagnetic field is represented by the complex amplitudes  $\mathbf{E}$  and  $\mathbf{H}$  (the time dependency is then omitted). In the case of two-dimensional structures,  $\mathbf{r}$  reduces to  $(x, y)$  and the fields do not depend on the  $z$  variable:  $\mathbf{E}(\mathbf{r}) = \mathbf{E}(x, y)$  and  $\mathbf{H} = \mathbf{H}(x, y)$ . Let  $\Omega$  denote the considered domain, a closed subset of  $\mathbb{R}^2$  of boundary  $\partial\Omega$ . The domain  $\Omega$  can be constituted of several sub-domains  $\Omega_j \in \Omega$  of boundary  $\partial\Omega_j$  such that  $\Omega = \cup\Omega_j$ . For each  $\Omega_j$ , let  $l_{\Omega_j}$  be the characteristic function:  $l_{\Omega_j}(\mathbf{r}) = 1$  if  $\mathbf{r} \in \Omega_j$  and  $l_{\Omega_j}(\mathbf{r}) = 0$  otherwise. Each sub-domain is made of a linear, possibly graded-index, isotropic, and non-magnetic material. The materials are assumed to be electrically frequency dispersive and dissipative. The tensor fields of relative complex permittivity  $\epsilon_j$  in each sub-domain  $\Omega_j$  are

$$\epsilon_j(\omega) = \epsilon_j(\omega) \mathbf{l}_d \quad (1)$$

and the relative permittivity  $\epsilon$  of the total structure can be written:

$$\epsilon(\omega, \mathbf{r}) = \sum_j l_{\Omega_j}(\mathbf{r}) \epsilon_j(\omega) \mathbf{l}_d. \quad (2)$$

It is assumed that the frequency dependence of each  $\epsilon_j$  can be modelled by:

$$\epsilon_j(\omega) = \epsilon_{\infty_j} - \sum_k \frac{\omega_{p,jk}^2}{\omega^2 + i\gamma_{D,jk}\omega - \omega_{D,jk}^2}, \quad (3)$$

which corresponds to a superposition of Lorentz resonances [1]. This model is known to be particularly relevant to the describe the permittivity of metals in the visible range [12]. Note that these functions of  $\omega$  are analytic in the upper half plane of complex frequencies and hence satisfy the causality requirement. It is stressed that purely dispersive causal systems (without absorption) can be tackled by setting the damping constant  $\gamma_{D,jk}$  to 0. Finally, a pure Drude contribution is obtained for  $\omega_{D,jk} = 0$ .

The goal of the present paper is to perform the spectral analysis of the Maxwell's equations which is based on the calculation of the eigenvalues and the associated eigenvectors of the source free equations:

$$\begin{aligned} \nabla \times \mathbf{E}(\omega, \mathbf{r}) &= i\omega\mu_0 \mathbf{l}_d \mathbf{H}(\omega, \mathbf{r}), \\ \nabla \times \mathbf{H}(\omega, \mathbf{r}) &= -i\omega\epsilon_0 \epsilon(\omega, \mathbf{r}) \mathbf{E}(\omega, \mathbf{r}), \end{aligned} \quad (4)$$

where  $\mu_0$  and  $\epsilon_0$  are the vacuum permeability and permittivity. These equations can be expressed as

$$\mathbf{M}_0(\omega, \mathbf{r}) \mathbf{F}_0(\omega, \mathbf{r}) = \omega \mathbf{F}_0(\omega, \mathbf{r}), \quad (5)$$

where

$$\mathbf{M}_0(\omega, \mathbf{r}) = \begin{bmatrix} 0 & i\epsilon^{-1}(\omega, \mathbf{r})/\epsilon_0 \nabla \times \\ -i/\mu_0 \nabla \times & 0 \end{bmatrix}, \quad (6)$$

and

$$\mathbf{F}_0(\omega, \mathbf{r}) = \begin{bmatrix} \mathbf{E}(\omega, \mathbf{r}) \\ \mathbf{H}(\omega, \mathbf{r}) \end{bmatrix}. \quad (7)$$

Here  $\omega$  appears clearly as the eigenvalue of the operator  $\mathbf{M}_0$  with its associated eigenvector  $\mathbf{F}_0$ . As already mentioned, in presence of dispersion, this EigenValue Problem (EVP) is non-linear in frequency since  $\mathbf{M}_0$  depends on  $\omega$ . When in addition absorption takes place, this operator  $\mathbf{M}_0$  is also non-hermitian, which requires a numerical computation in the plane of complex frequencies.

### B. The auxiliary fields formalism and resonance formalism.

The auxiliary fields formalism has been introduced and developed by A. Tip since 1997 [10, 11]. It is based on the adjunction of auxiliary fields to the classical electromagnetic field that leads to the construction of the unique hermitian extension [13] of the Maxwell's operator which is linear in frequency. In this paper, the purely dispersive case introduced in [14] is extended to Drude-Lorentz resonances with absorption, see Eq. (3). This extended formalism, called "resonance" formalism, is derived hereafter (and in the appendix). A similar technique has been used in [9] to compute the photonic band structure of "metallic" 2D square rods.

#### 1. Single Drude-Lorentz resonance.

A relative permittivity given by a single Drude-Lorentz resonance is considered:

$$\epsilon(\omega) = \epsilon_{\infty} - \frac{\omega_p^2}{\omega^2 + i\gamma_D \omega - \omega_D^2}. \quad (8)$$

Defining  $\omega_r = \sqrt{\omega_D^2 - \gamma_D^2/4}$ ,  $\omega_{\pm} = \pm\omega_r - i\gamma_D/2$ , and the two following auxiliary fields,

$$\mathbf{A}_L^{\pm}(\mathbf{r}, t) = \mp i \frac{\omega_p \omega_{\pm}}{\omega_r \sqrt{2}} \int_{-\infty}^t ds \exp[-i\omega_{\pm}(t-s)] \mathbf{E}(\mathbf{r}, s), \quad (9)$$

Maxwell's equations become in the time regime (see Appendix VIA):

$$\begin{aligned} \epsilon_0 \epsilon_{\infty} \frac{\partial \mathbf{E}}{\partial t}(\mathbf{r}, t) &= \nabla \times \mathbf{H}(\mathbf{r}, t) - i \frac{\omega_p}{\sqrt{2}} \epsilon_0 [\mathbf{A}_L^+(\mathbf{r}, t) + \mathbf{A}_L^-(\mathbf{r}, t)], \\ \mu_0 \frac{\partial \mathbf{H}}{\partial t}(\mathbf{r}, t) &= -\nabla \times \mathbf{E}(\mathbf{r}, t), \\ \frac{\partial \mathbf{A}_L^{\pm}}{\partial t}(\mathbf{r}, t) &= \mp i \frac{\omega_p \omega_{\pm}}{\sqrt{2} \omega_r} \mathbf{E}(\mathbf{r}, t) - i\omega_{\pm} \mathbf{A}_L^{\pm}(\mathbf{r}, t). \end{aligned} \quad (10)$$

As to the harmonic regime, it is deduced from a Fourier decomposition with respect to time:

$$\begin{aligned}
-i\omega\epsilon_0\epsilon_\infty\mathbf{E}(\mathbf{r},\omega) &= \nabla \times \mathbf{H}(\mathbf{r},\omega) \\
&\quad -i\frac{\omega_p}{\sqrt{2}}\epsilon_0 [\mathbf{A}_L^+(\mathbf{r},\omega) + \mathbf{A}_L^-(\mathbf{r},\omega)], \\
-i\omega\mu_0\mathbf{H}(\mathbf{r},\omega) &= -\nabla \times \mathbf{E}(\mathbf{r},\omega), \\
-i\omega\mathbf{A}_L^\pm(\mathbf{r},\omega) &= \mp i\frac{\omega_p\omega_\pm}{\sqrt{2}\omega_r} \mathbf{E}(\mathbf{r},\omega) - i\omega_\pm\mathbf{A}_L^\pm(\mathbf{r},\omega).
\end{aligned} \tag{11}$$

This last set of equations can be summarized as

$$\mathbf{M}(\mathbf{r})\mathbf{F}(\omega, \mathbf{r}) = \omega\mathbf{F}(\omega, \mathbf{r}), \tag{12}$$

using the following matrix and vector notations:

$$\mathbf{M}(\mathbf{r}) = \begin{bmatrix} 0 & \frac{i}{\epsilon_0\epsilon_\infty}\nabla \times & \frac{\omega_p}{\sqrt{2}\epsilon_\infty} & \frac{\omega_p}{\sqrt{2}\epsilon_\infty} \\ -i/\mu_0\nabla \times & 0 & 0 & 0 \\ \frac{\omega_p}{\sqrt{2}\omega_r}\omega_+ & 0 & \omega_+ & 0 \\ -\frac{\omega_p}{\sqrt{2}\omega_r}\omega_- & 0 & 0 & \omega_- \end{bmatrix}, \tag{13}$$

and

$$\mathbf{F}(\omega, \mathbf{r}) = \begin{bmatrix} \mathbf{E}(\omega, \mathbf{r}) \\ \mathbf{H}(\omega, \mathbf{r}) \\ \mathbf{A}_L^+(\omega, \mathbf{r}) \\ \mathbf{A}_L^-(\omega, \mathbf{r}) \end{bmatrix}. \tag{14}$$

It is important to notice that the operator  $\mathbf{M}(\mathbf{r})$  in Eq. (13) is frequency independent.

## 2. Single Drude resonance.

Let the relative permittivity now be given by the Drude model:

$$\epsilon(\omega) = \epsilon_\infty - \frac{\omega_p^2}{\omega(\omega + i\gamma_D)}. \tag{15}$$

In this case, a single auxiliary field is defined as

$$\mathbf{A}_D(\mathbf{r}, t) = -2i\frac{\omega_p}{\sqrt{2}} \int_{-\infty}^t ds \exp[-\gamma_D(t-s)]\mathbf{E}(\mathbf{r}, s). \tag{16}$$

Thus, Maxwell's equations in the time regime are

$$\begin{aligned}
\epsilon_0\epsilon_\infty \frac{\partial \mathbf{E}}{\partial t}(\mathbf{r}, t) &= \nabla \times \mathbf{H}(\mathbf{r}, t) - i\frac{\omega_p\epsilon_0}{\sqrt{2}}\mathbf{A}_D(\mathbf{r}, t), \\
\mu_0 \frac{\partial \mathbf{H}}{\partial t}(\mathbf{r}, t) &= -\nabla \times \mathbf{E}(\mathbf{r}, t), \\
\frac{\partial \mathbf{A}_D}{\partial t}(\mathbf{r}, t) &= -2i\frac{\omega_p}{\sqrt{2}}\mathbf{E}(\mathbf{r}, t) - \gamma_D\mathbf{A}_D(\mathbf{r}, t).
\end{aligned} \tag{17}$$

In the time harmonic regime, they become

$$\begin{aligned}
-i\omega\epsilon_0\epsilon_\infty\mathbf{E}(\mathbf{r},\omega) &= \nabla \times \mathbf{H}(\mathbf{r},\omega) - i\frac{\omega_p\epsilon_0}{\sqrt{2}}\mathbf{A}_D(\mathbf{r},\omega), \\
-i\omega\mu_0\mathbf{H}(\mathbf{r},\omega) &= -\nabla \times \mathbf{E}(\mathbf{r},\omega), \\
-i\omega\mathbf{A}_D(\mathbf{r},\omega) &= -2i\frac{\omega_p}{\sqrt{2}}\mathbf{E}(\mathbf{r},\omega) - \gamma_D\mathbf{A}_D(\mathbf{r},\omega).
\end{aligned} \tag{18}$$

Finally, a compact expression is obtained as previously using vector and matrix notations:

$$\mathbf{M}(\mathbf{r})\mathbf{F}(\omega, \mathbf{r}) = \omega\mathbf{F}(\omega, \mathbf{r}), \tag{19}$$

where

$$\mathbf{M}(\mathbf{r}) = \begin{bmatrix} 0 & \frac{i}{\epsilon_0\epsilon_\infty}\nabla \times & \frac{\omega_p}{\sqrt{2}\epsilon_\infty} \\ -\frac{i}{\epsilon_0\epsilon_\infty}\nabla \times & 0 & 0 \\ \frac{\mu_0\omega_p}{2\sqrt{2}} & 0 & -i\gamma_D \end{bmatrix}, \tag{20}$$

and

$$\mathbf{F}(\omega, \mathbf{r}) = \begin{bmatrix} \mathbf{E}(\omega, \mathbf{r}) \\ \mathbf{H}(\omega, \mathbf{r}) \\ \mathbf{A}_D(\omega, \mathbf{r}) \end{bmatrix}. \tag{21}$$

## 3. Superposition of Drude and Drude-Lorentz resonances.

For the general case of a sum of Drude and Drude-Lorentz resonances as in Eq. (3), the same reasoning leads to the adjunction of a couple of auxiliary fields defined as in Eq. (9) for each Drude-Lorentz resonance, and of a single auxiliary field defined as in Eq. (16) for each Drude resonance.

## 4. Formalism for a multidomain structure.

When several dispersive materials are involved in the total structure  $\Omega$ , the parameters defined in the previous sections (*e.g.*  $\epsilon_\infty$ ,  $\omega_p$ ,  $\omega_r$ ,  $\gamma_D$  for a single Drude-Lorentz resonance) take different constant values in the different subdomains  $\Omega_j$ . It is then possible to define those parameters (here for example  $\epsilon_\infty$ ) as a function of space:

$$\epsilon_\infty(\mathbf{r}) = \sum_j \mathbf{1}_{\Omega_j}(\mathbf{r})\epsilon_{\infty_j} \tag{22}$$

and so on for all the parameters involved in the chosen permittivity model.

## C. Finite element formulation

In this section, the FEM formulation is adapted to the resonance formalism in the frame of a single Lorentz resonance. Here, the two auxiliary fields  $\mathbf{A}_L^+$  and  $\mathbf{A}_L^-$  defined in Eq. (9) are introduced. Note that the spatial dependency of all the parameters of the Drude-Lorentz resonance in the resonance formalism frame is omitted [*e.g.*  $\epsilon_\infty = \epsilon_\infty(\mathbf{r})$ ].

The usual treatment of 2D non-conical mount (also called scalar) electromagnetic problems, consists in choosing for unknown the out-of-plane component of the

electric or magnetic fields which is conveniently continuous everywhere. Two linear polarization cases are traditionally considered, s-polarization [electric field along the z-direction:  $\mathbf{E} = E_z(x, y)\mathbf{z}$ ] and p-polarization [magnetic field along the z-direction:  $\mathbf{H} = H_z(x, y)\mathbf{z}$ ]. Maxwell's equations are combined to form one scalar Helmholtz propagation equation involving  $E_z$  or  $H_z$  solely.

The generalized Maxwell eigenvector  $\mathbf{F}$  in the general case of Eq. (9) contains four vector fields belonging to the same function space. However, in two dimensions, the seemingly obvious choice of nodal elements for the discretize the continuous electric field  $\mathbf{E} = E_z(x, y)\mathbf{z}$  together with edge elements to discretize the in-plane discontinuous magnetic field  $\mathbf{H} = H_x(x, y)\mathbf{x} + H_y(x, y)\mathbf{y}$  is not appropriate. Indeed,  $\mathbf{E}$  and  $\mathbf{H}$  would not be evaluated at the same points, since the physical quantity associated to edge elements unknowns is the circulation of the electric field along the edges of one mesh triangle, whereas the physical quantity associated to nodal elements unknowns is the very value of the field at one node of the mesh. Hence,  $\mathbf{E}$  and corresponding  $\mathbf{H}$  would, in fact, not be evaluated at the same points. Keeping the full system Eq. (9) would require the notion of dual grid, as the interlaced cubic Yee grid [15] for instance, or the use of mixed finite elements. The choice was made here to work with one element family only by classically removing  $\mathbf{H}$  from the equation system. However, a quadratic EVP is obtained:

$$\omega^2 \epsilon_\infty \mathbf{E}(\mathbf{r}, \omega) = c^2 \nabla \times \nabla \times \mathbf{E}(\mathbf{r}, \omega) + \omega \frac{\omega_p}{\sqrt{2}} [\mathbf{A}_L^+(\mathbf{r}, \omega) + \mathbf{A}_L^-(\mathbf{r}, \omega)], \quad (23)$$

$$\omega \mathbf{A}_L^+(\mathbf{r}, \omega) = \frac{\omega_p \omega_+}{\sqrt{2} \omega_r} \mathbf{E}(\mathbf{r}, \omega) + \omega_+ \mathbf{A}_L^+(\mathbf{r}, \omega), \quad (24)$$

$$\omega \mathbf{A}_L^-(\mathbf{r}, \omega) = -\frac{\omega_p \omega_-}{\sqrt{2} \omega_r} \mathbf{E}(\mathbf{r}, \omega) + \omega_- \mathbf{A}_L^-(\mathbf{r}, \omega). \quad (25)$$

This choice is possible thanks to recent advances in linear algebra algorithms that provided efficient libraries able to directly tackle such quadratic EVP [16]. The weak form of this last equation system is classically obtained by projecting the unknown vector fields on weighted vectors fields  $\mathbf{W}'$  and integrating over the support of the unknowns,  $\Omega$  for  $\mathbf{E}$  and  $\Omega'$  for auxiliary fields  $\mathbf{A}_L^+$  and  $\mathbf{A}_L^-$ , leading to the following residue:

$$\begin{aligned} \int_{\Omega} d\Omega \quad & -\omega^2 \epsilon_\infty \mathbf{E} \cdot \overline{\mathbf{W}'} + c^2 \nabla \times \nabla \times \mathbf{E} \cdot \overline{\mathbf{W}'} \\ & + \omega \frac{\omega_p}{\sqrt{2}} [\mathbf{A}_L^+ + \mathbf{A}_L^-] \cdot \overline{\mathbf{W}'} \\ + \int_{\Omega'} d\Omega' \quad & -\omega \mathbf{A}_L^+ \cdot \overline{\mathbf{W}'} + \frac{\omega_p \omega_+}{\sqrt{2} \omega_r} \mathbf{E} \cdot \overline{\mathbf{W}'} \\ & + \omega_+ \mathbf{A}_L^+ \cdot \overline{\mathbf{W}'} \\ & -\omega \mathbf{A}_L^- \cdot \overline{\mathbf{W}'} - \frac{\omega_p \omega_-}{\sqrt{2} \omega_r} \mathbf{E} \cdot \overline{\mathbf{W}'} \\ & + \omega_- \mathbf{A}_L^- \cdot \overline{\mathbf{W}'} . \end{aligned} \quad (26)$$

Integrating by parts Eq. (26) and using the Green-Ostrogradsky theorem leads to:

$$\begin{aligned} \int_{\Omega} d\Omega \quad & -\omega^2 \epsilon_\infty \mathbf{E} \cdot \overline{\mathbf{W}'} + c^2 \nabla \times \mathbf{E} \cdot \nabla \times \overline{\mathbf{W}'} \\ & + \omega \frac{\omega_p}{\sqrt{2}} [\mathbf{A}_L^+ + \mathbf{A}_L^-] \cdot \overline{\mathbf{W}'} \\ + \int_{\Omega'} d\Omega' \quad & -\omega \mathbf{A}_L^+ \cdot \overline{\mathbf{W}'} + \frac{\omega_p \omega_+}{\sqrt{2} \omega_r} \mathbf{E} \cdot \overline{\mathbf{W}'} \\ & + \omega_+ \mathbf{A}_L^+ \cdot \overline{\mathbf{W}'} \\ & -\omega \mathbf{A}_L^- \cdot \overline{\mathbf{W}'} - \frac{\omega_p \omega_-}{\sqrt{2} \omega_r} \mathbf{E} \cdot \overline{\mathbf{W}'} \\ & + \omega_- \mathbf{A}_L^- \cdot \overline{\mathbf{W}'} \\ - \int_{\partial\Omega} dS \quad & (\nabla \times \mathbf{E} \times \mathbf{n}) \cdot \overline{\mathbf{W}'} . \end{aligned} \quad (27)$$

where  $\mathbf{n}$  refers to the exterior unit vector to the surface  $\partial\Omega$  enclosing  $\Omega$ . The last surface term in Eq. (27) is used to impose boundary conditions (Dirichlet, Neumann or Bloch-Floquet conditions [17]). Note that no particular attention needs to be paid to the auxiliary fields on the boundary of  $\Omega'$ .

As previously mentioned, two cases of polarization are considered (s and p). In s-polarization, the electric field and indeed the auxiliary fields have only one component along the  $O_z$  axis. The problem is scalar and nodal first order elements are used as a basis for the unknowns. In p-polarization, the fields have two possibly discontinuous components in the plane of invariance  $O_{xy}$ . The use of edge elements (or Whitney forms) is necessary [18]. These edge elements naturally take into account the discontinuity of the normal component of the electric field across interfaces. According to the Galerkin formulation, these basis functions are also used as weighted functions  $\mathbf{W}'$ .

The described weak formulation has been implemented in practice into the FEM freewares Gmsh [19] for mesh generation and visualization, and GetDP [20] as a Finite Element library.

### III. NUMERICAL VALIDATION OF THE METHOD.

The validity of the method is tested in the case of a two-dimensional closed cavity made of two square domains  $\Omega_1$  and  $\Omega_2$ , with sides denoted by  $a$ , and filled with materials of relative permittivity  $\epsilon_1(\omega)$  and  $\epsilon_2(\omega)$  (see Fig. 1). The cavity is delimited by a perfectly conducting metal, with the corresponding conditions at the cavity boundary  $\partial\Omega$ .

The complex resonances  $\omega_n$  of this structure can be determined by solving the following transcendental equation defining the dispersion law (see Appendix VIB for the derivation of the dispersion equation):

$$\frac{\tan[\beta_1(\omega_n)a]}{\beta_1(\omega_n)} + \frac{\tan[\beta_2(\omega_n)a]}{\beta_2(\omega_n)} = 0 \quad (28)$$

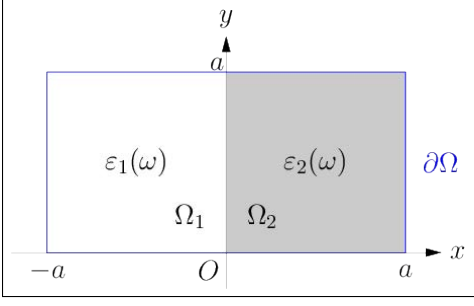


FIG. 1. Scheme of the considered closed cavity.

for s-polarization and

$$\frac{\beta_1(\omega_n)}{\epsilon_1(\omega_n)} \tan[\beta_1(\omega_n)a] + \frac{\beta_2(\omega_n)}{\epsilon_2(\omega_n)} \tan[\beta_2(\omega_n)a] = 0 \quad (29)$$

for p-polarization. Here the complex functions of  $\omega$ ,  $\beta_1$  and  $\beta_2$ , are defined by

$$\beta_j(\omega_n) = \sqrt{\frac{\omega_n^2}{c^2} \epsilon_j(\omega_n) - \frac{q^2 \pi^2}{a^2}}, \quad j \in \{1, 2\}, \quad (30)$$

where  $q \in \mathbb{N} \setminus \{0\}$  for s-polarization and  $q \in \mathbb{N}$  for p-polarization.

The considered cavity has been implemented into the FEM modal method described in Sec. II C. with the permittivities  $\epsilon_1 = 2.0$  (*i.e.* a non dispersive material) and

$$\epsilon_2(\omega) = \epsilon_\infty - \frac{\omega_p^2}{\omega^2 + \gamma i \omega - \omega_0^2}, \quad (31)$$

with

$$\epsilon_\infty = 3.0, \quad \frac{\omega_p a}{2\pi c} = 1.2, \quad \frac{\gamma a}{2\pi c} = 0.2, \quad \frac{\omega_0 a}{2\pi c} = 0.6. \quad (32)$$

As the problem is formulated with the electric field, Dirichlet boundary conditions are imposed on the boundary  $\partial\Omega$  of the structure. Hence, the eigenfrequencies of the structure for both s- and p-polarizations are now determined in two different ways: using a numerical resolution of the transcendental dispersion equations (28) and (29) and the FEM modal method. The comparison between the results of the two methods is shown in Fig. 2 for s- (top panel) and p-polarization (bottom). The results show excellent agreement for s-polarization. In both s and p polarizations, a first branch of modes is observed to be converging towards the (normalized) frequency  $(\omega_1 a)/(2\pi c) \simeq 0,59 - 0.1i$  which corresponds to the pole frequency in the expression (31):  $|\epsilon(\omega)| \rightarrow \infty$  when  $\omega \rightarrow \omega_1$ . It is also observed that the spectrum of resonances tends to the real axis at high frequencies. Indeed, in this range, the value of the permittivity  $\epsilon_2(\omega)$  tends to  $\epsilon_\infty = 3.0$ , and the spectrum of a system with purely real and positive permittivity is retrieved. For p-polarization, a second branch of modes appears with an accumulation point at the (normalized) frequency  $(\omega_2 a)/(2\pi c) \simeq 0.8 - 0.1i$  where  $\epsilon_2(\omega) = -\epsilon_1$ .

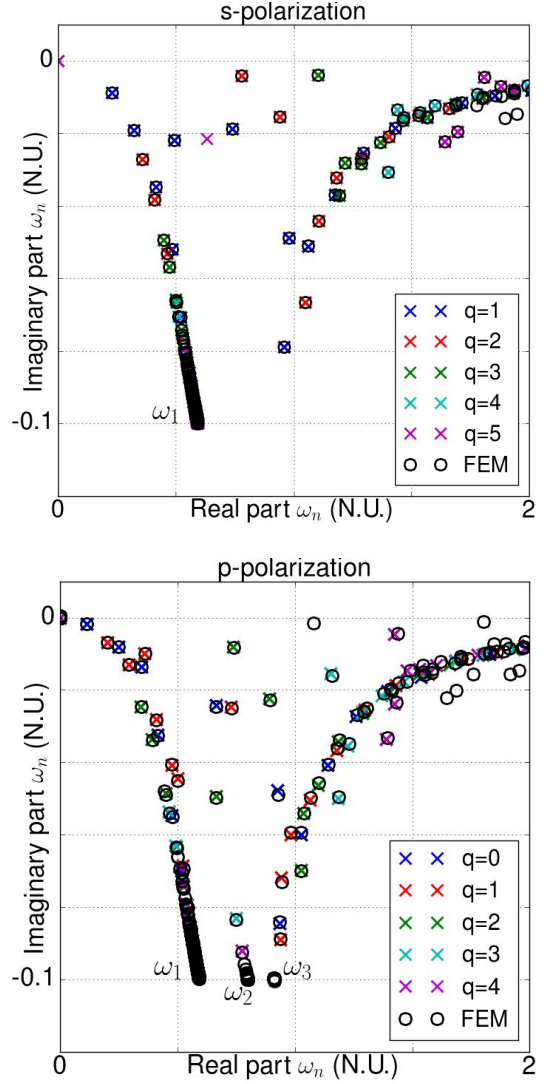


FIG. 2. Comparison between the results obtained using the FEM method with auxiliary fields and the semi-analytical method for s- and p-polarization.

This branch corresponds to the surface plasmon modes (see bottom panel in Fig. 2 and left panel in Fig. 3).

For p polarization, spurious modes are also observed around  $(\omega_3 a)/(2\pi c) \simeq 0.91 - 0.1i$  which corresponds to the frequency where  $\epsilon_2(\omega) = 0$ . The presence of these spurious modes can be explained by the fact that, when  $\epsilon_2(\omega) = 0$ , the divergence free condition of the electric field  $\nabla \cdot [\epsilon \mathbf{E}] = 0$  fails since  $\mathbf{E}$  can take any value in the dispersive media with  $\epsilon_2(\omega) = 0$ . As a consequence, the precision of the results is affected by the presence of these spurious modes and the accuracy of the FEM results is degraded in a neighborhood of  $\omega_3$ , which probably has overlap with the branch of surface plasmon modes around  $\omega_2$  (cf Fig. 3, right panel). These spurious modes are not present in s polarization as the electric field is oriented along the  $O_z$  axis and spatially depends only on  $(x, y)$  so that the divergence free condition is included in the scalar

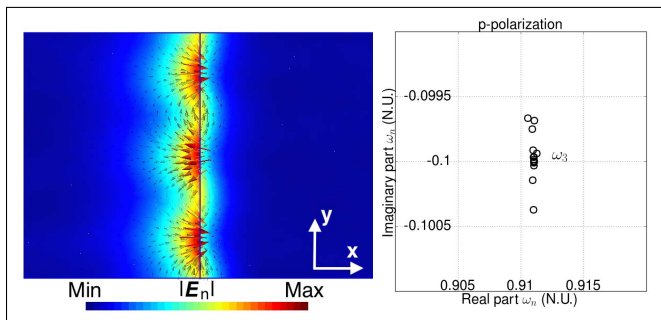


FIG. 3. Left panel: Electric field for one mode of the surface plasmon branch in p-polarization at the frequency  $\omega_a/(2\pi c) = 0.748 - 0.083i$ . Right panel: Zoom on the spectra of Fig.2 around the spurious modes produced by the  $\epsilon(\omega) = 0$  at  $\omega = \omega_3$ .

equation. These spurious modes can be avoided by the implementation of Lagrangian preconditioners into the eigenvalue problem solver.

In addition, it is mentioned that the method has also been validated in the case of two dispersive domains with relative permittivities given by a sums of Drude and Drude-lorentz resonances. This final test shows that the proposed method can be used in practical situations.

The numerical method presented in this paper provides an efficient tool to compute and analyze the complex spectrum of dispersive systems, and thus it opens new possibilities of investigations in the area of non self-adjoint operators which has been rarely explored. The situation of a two-dimensional crystal is considered in the next section.

#### IV. COMPLEX RESONANCES IN A TWO DIMENSIONAL PHOTONIC CRYSTAL

The two dimensional photonic crystals considered in previous articles [2, 3] are investigated. The crystals are square arrays with lattice constant  $a$  along the  $O_x$  and  $O_y$  axis, with square or circular rods made of a Drude metal and embedded in air (see Fig.4). As the structure we are

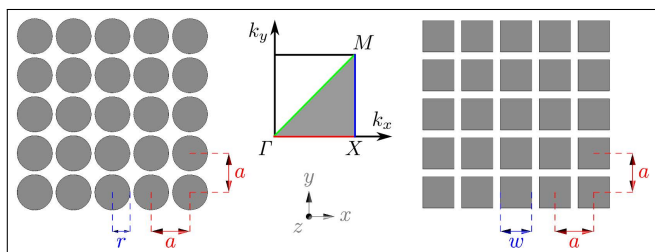


FIG. 4. Scheme of the modeled 2D photonic crystals in one invariance plane and the associated first reduced Brillouin zone (triangle  $\Gamma XM$ :  $\Gamma X$  in red,  $\Gamma M$  in green, and  $XM$  in blue).

dealing with is bi-periodic in the  $xy$  plane, Bloch-Floquet

(or quasi-periodicity) conditions [17] are imposed on the  $x$  and  $y$  boundary of the square unit cell thanks to the surface term of Eq.27. These quasi-periodic boundary conditions are defined by the Bloch wvector  $\mathbf{k} = k_x \mathbf{x} + k_y \mathbf{y}$  of the electromagnetic eigenmodes. Notice that the components  $(k_x, k_y)$  of the wvector  $\mathbf{k}$  are real while the eigenfrequencies are complex. The modal analysis of the structure cell is thus performed through the FEM described in Sec. 2.II C, where Bloch vector  $\mathbf{k}$  is fixed as a parameter spanning the first reduced Brillouin zone.

The dielectric relative permittivity of the rods is given by the single Drude resonance:

$$\epsilon(\omega) = 1 - \frac{\omega_p^2}{\omega(\omega + i\gamma)}, \quad (33)$$

with

$$\frac{\omega_p a}{2\pi c} = 1.1, \quad \frac{\gamma a}{2\pi c} = 0.05. \quad (34)$$

The width and radius of the rods have been chosen so that the filling fraction of the structures is equal to 0.65 in both cases, *i.e.*  $w = 0.806 a$  in case of square rods and  $r = 0.455 a$  in case of circular rods. The eigenfrequencies of the structures are retrieved for all wvectors  $\mathbf{k}$  lying in the first reduced Brillouin zone of the considered crystals ( $k_x \in [0, \pi/a]$  and  $k_y \in [0, k_x]$ ) as represented in Fig. 4.

#### A. Resonances for s-polarization

Fig. 5 shows the whole spectrum of the photonic crystals made of square (top panel) and circular (bottom panel) rods for s-polarization. The result of this simulation confirms previous results of the literature obtained with completely different methods. The exact modal method [21] is used in Ref. [2] for square rods, while an expansion on cylindrical harmonics combined with lattice sums is used in Ref. [3] for circular rods. Notice that the set of resonances tends to the spectrum of the free Laplacian at high frequencies (see Fig. 5) according to the behavior of the permittivity in this range ( $|\epsilon(\omega)| \rightarrow 1$  when  $|\omega| \rightarrow \infty$ ). Also, the complex spectra of the two crystals with square and circular rods turn out to be similar, as confirmed by Fig. 6 showing the first band of complex resonances. Hence, from now on, the investigation is focused on the crystal made of square rods.

Fig. 7 shows bands 2 and 3 and confirms results presented in reference [2] where the complex resonances have been rigorously defined and calculated using perturbation theory. Fig. 8 shows the bands 4 and 5 (and higher) which have even richer structures. As pointed out in [3], calculations of band structures are generally performed for wvector  $\mathbf{k}$  spanning the boundary of the first reduced Brillouin zone (in colors on Fig. 4), the general assumption being that the spectrum of complex resonances is located inside the contour formed by the complex resonances corresponding to this boundary. Figure 8 shows

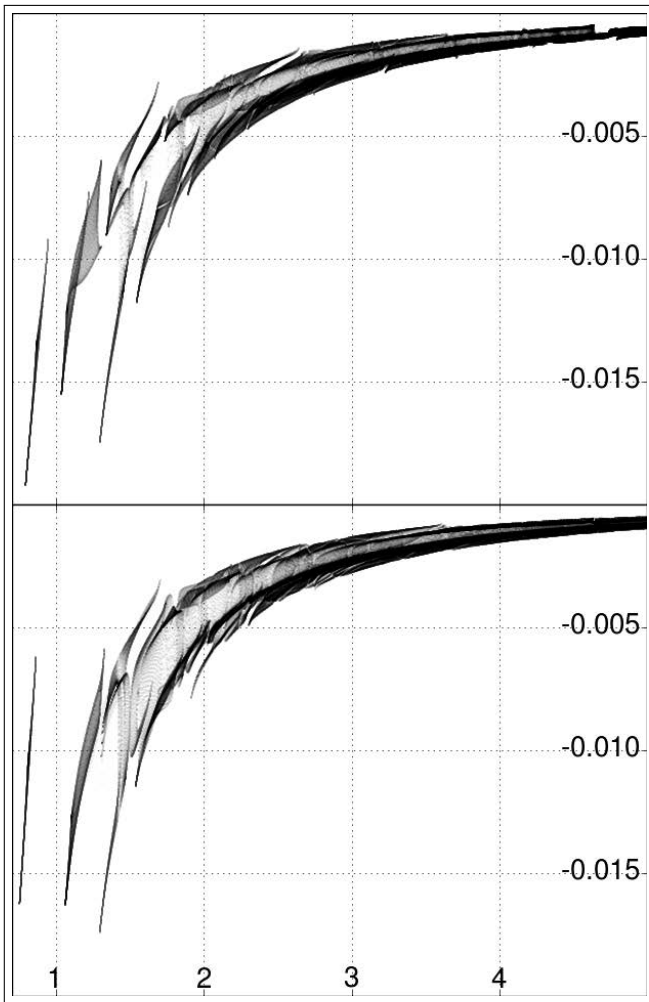


FIG. 5. Spectra of the normalized eigenfrequencies  $\omega_n a / (2\pi c)$  of the photonic crystal of square (top panel) and circular (bottom panel) rods for all the wavevectors  $\mathbf{k}$  in the first Brillouin zone.

a counterexample of this assumption where it can be observed that some resonances are located outside those deformed triangles, which confirms results obtained in [3] for circular rods. Moreover, Fig. 8 reveals that two different bands (bands 4 and 5) are connected with a set of eigenfrequencies. Similar behaviors are observed for higher order bands.

In order to have a better understanding of these spectra, the complex resonances are represented for wavevector  $\mathbf{k}$  along the four “iso- $k_y$ ” lines defined by setting the  $k_y$  component to the following fixed values:  $0.23\pi/a$ ,  $0.24\pi/a$ ,  $0.37\pi/a$ , and  $0.38\pi/a$ , while the  $k_x$  component spans segments  $[k_y, 0.5\pi/a]$ .

Left panel of Fig. 9 shows iso- $k_y$  lines in the connected bands 4 and 5 corresponding to Fig. 8. For  $k_y = 0.23\pi/a$ , the path followed by the resonances (red dots) starts from the side of the deformed triangle corresponding to  $XM$  (blue diamonds), then goes out the deformed triangle, and finally comes back to the other side of the deformed

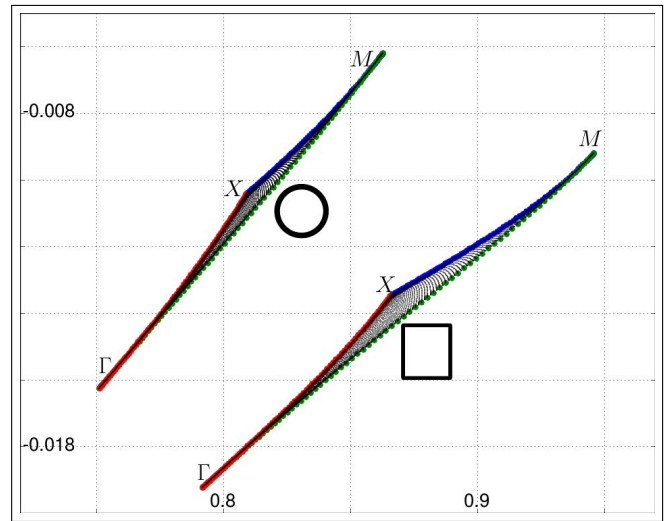


FIG. 6. First band of the spectra of the normalized eigenfrequencies  $\omega_n a / (2\pi c)$ .

triangle corresponding to  $\Gamma M$  (green diamonds). The part of the path leaving the deformed triangle takes the shape of a sharp dip for the lower absorption band and the shape of a sharp peak for the higher absorption band. Hence these dip and peak attract seemingly each other. For  $k_y = 0.24\pi/a$ , the path followed by the resonances (green dots) starts from the side of the first deformed

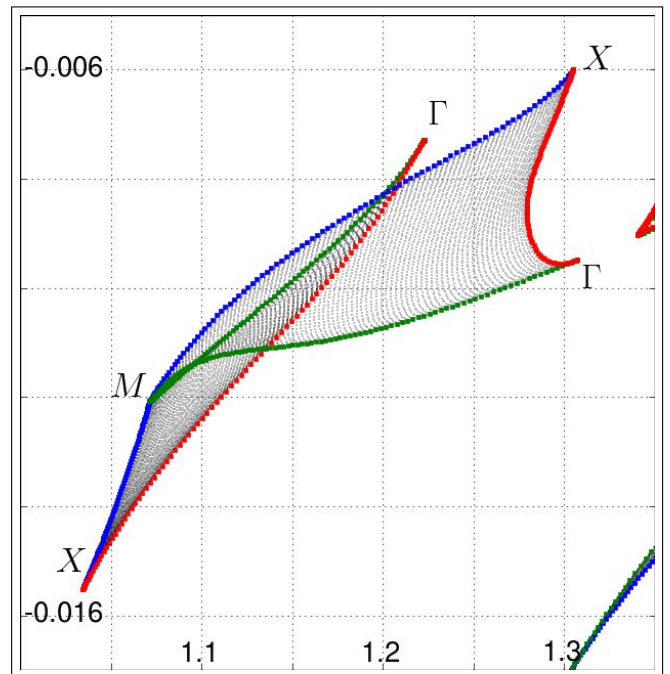


FIG. 7. Second and third bands of the spectrum of the normalized resonances  $\omega_n a / (2\pi c)$ . The resonances corresponding to the three boundaries of the triangular reduced first Brillouin zone are drawn with colors:  $\Gamma X$  in red,  $\Gamma M$  in green, and  $XM$  in blue.

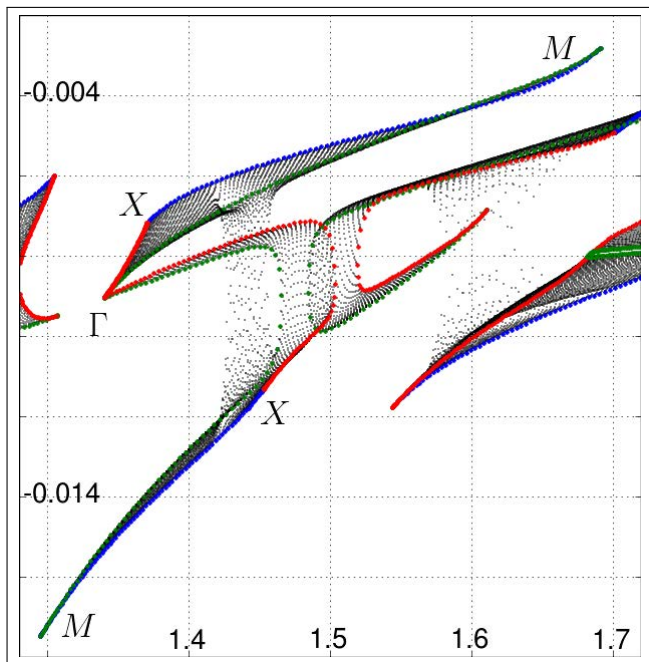


FIG. 8. Band 4, band 5 and of higher order of the spectra of the normalized eigenfrequencies  $\omega_n a / (2\pi c)$ . The resonances corresponding to the three boundaries of the triangular reduced first Brillouin zone are drawn with colors:  $\Gamma X$  in red,  $\Gamma M$  in green, and  $XM$  in blue.

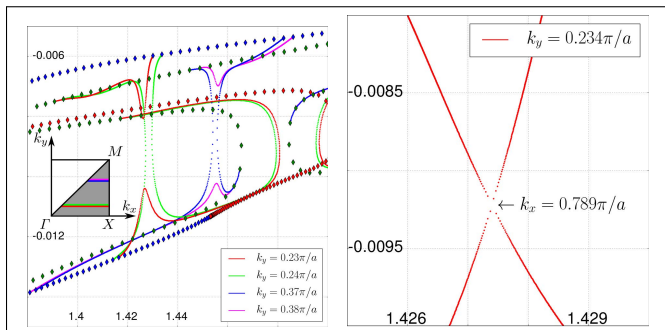


FIG. 9. Left panel: Resonances in the photonic crystal made of Drude square rods for several iso- $k_y$  lines in bands 4 and 5. Left panel: Zoom in the area around the critical point  $(k_x, k_y) \approx (0.789, 0.234)\pi/a$  in the band structure.

triangle corresponding to  $XM$  (blue diamonds), goes out this first deformed triangle to reach the side of the second deformed triangle (side corresponding to  $\Gamma M$ , green diamonds). For this value  $k_y = 0.24\pi/a$  the two bands are connected. Similar observations can be done for values of  $k_y$  fixed to  $0.38\pi/a$  (violet dots in Fig. 9 showing a dip and a peak) and  $0.37\pi/a$  (blue dots showing connexion). Therefore, it can be concluded that in a range of wavevectors the bands 4 and 5 are enlaced, see Fig. 11 for a representation of the interlacing. Also, it is stressed that the critical wavevector at which the peak and the dip touch each other at just one point may be associated to singular properties. Right panel of 9 shows the resonances for

iso- $k_y$  lines around this critical point, whose wavevector has been estimated around  $(k_x, k_y) \approx (0.789, 0.234)\pi/a$ .

Fig. 10 shows iso- $k_y$  lines in bands of higher order for  $k_y$  fixed to values  $0.23\pi/a$ ,  $0.24\pi/a$ ,  $0.37\pi/a$ , and  $0.38\pi/a$ . The path followed by the resonances exhibits

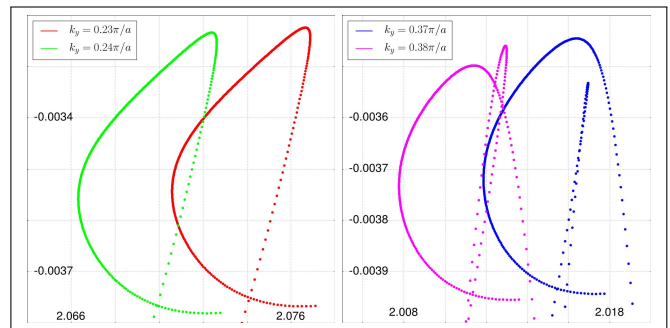


FIG. 10. Resonances in the photonic crystal made of Drude square rods for several iso- $k_y$  lines in bands of higher order showing loops (left) and cusps (right).

some loops (left panel) and cusps (right panel) when  $k_x$  spans  $[k_y, \pi/a]$ . These loops and cusps may have important effect on the complex group velocity defined as  $(\partial\omega)/(\partial k_x)$  with changes of direction.

Finally the connection between the two bands 4 and 5 observed in the previous figures is discussed. First, it is stressed that the resonances corresponding the Brillouin contour (i.e. the contour of the reduced Brillouin zone) describe some deformed triangles which do not contain all the resonances corresponding to the whole reduced Brillouin zone. Hence the description of the solely Brillouin contour does not provide all the information of the system: In particular, the critical point highlighted in Fig. 9 is precisely located in the inner of the reduced Brillouin zone. Fig. 11 proposes a representation of a band interlaced with a second one, as occurs for band 4 with band 5. This representation shows that the set of resonances corresponding to the Brillouin contour is not a closed path, but a deformed triangle with a cut and a segment. This cut in the deformed triangle defines two branches starting from the critical point defined above. Hence the inside of the Brillouin zone contains two critical points and two branches which may have particular properties. This observation supports the relevance of a scan of the whole reduced Brillouin zone for some systems.

Next, it is stressed that the interlacing of bands 4 and 5 may be interpreted as a coupling effect. In this case, it can be expected that the coupling of the two modes with the same frequency  $\omega$  and wavevector  $\mathbf{k}$  results from a symmetry which has been broken. In the present photonic crystal, no spatial symmetry is broken. However, in the Drude model (15), the resonances of the permittivity have not the same imaginary part with a first resonance at  $\omega = 0$  and a second at  $\omega = -i\gamma_D$ . Hence, one can imagine that this could break some symmetry in the time domain since other models for permittivity are

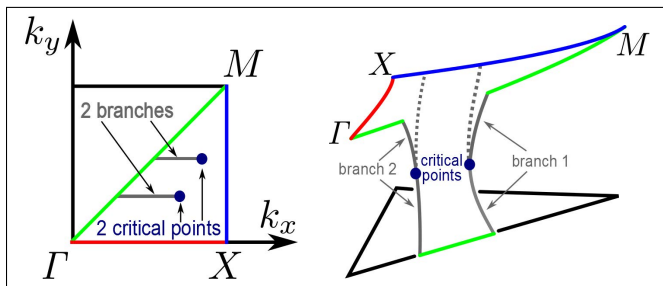


FIG. 11. Representation of the interlacing of the bands

generally made by couple of resonances  $\pm\omega_0 - i\gamma$  (with both  $\omega_0$  and  $\gamma$  real) with the same imaginary part. Such assumption is consistent with the interlacing observed in Figs. 8 and 9 which is essentially in the vertical (imaginary) direction in order to connect a low absorption band to a high absorption band.

This assumption can be checked by considering the resonances in the same crystal with square rods but with the permittivity now given by the Drude-Lorentz model (31) with the parameters

$$\epsilon_\infty = 1.0, \quad \frac{\omega_p a}{2\pi c} = 1.1, \quad \frac{\gamma a}{2\pi c} = 0.05, \quad \frac{\omega_0 a}{2\pi c} = 1.1. \quad (35)$$

The corresponding spectrum of resonances represented on Fig. 12 shows that the bands remain enlaced. Hence we conclude that the interlacing of bands is not produced by a broken symmetry in this kind of situation: further investigations are needed in a future work to understand this phenomenon.

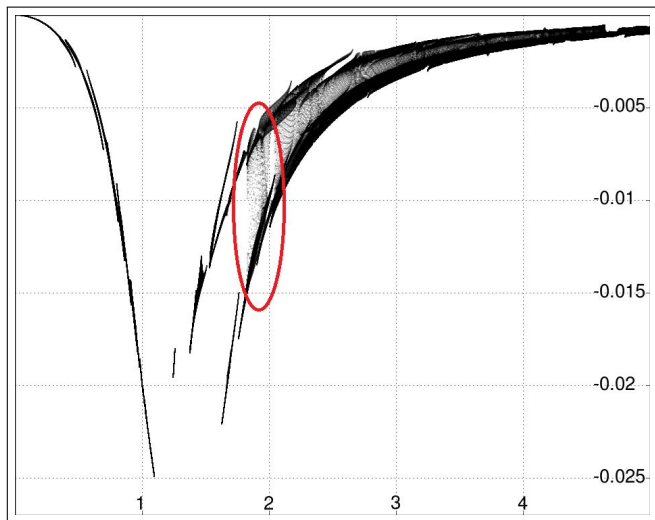


FIG. 12. Resonances in the photonic crystal made of Drude-Lorentz square rods. The highlighted area shows interlacing of bands.

## B. Resonances for p-polarization

The same numerical calculations have been performed for p-polarization with Drude parameters given by (33) and (34). In this case only the photonic crystal of circular rods is considered in order to compare the results to the one of the literature [3]. Fig. 13 presents the whole spectrum of complex resonances.

The results are in agreement with the ones in the literature [3], except for the presence of spurious modes as previously observed for closed cavities in Sec. 3. These spurious modes affect the results around the complex frequency  $\omega_3 \simeq 1, 1 - 0.025i$  where  $\epsilon(\omega_3) = 0$ . Notice that these spurious modes are mostly located on a vertical axis starting from the vanishing frequency  $\omega_3$  (red line on Fig. 13). In addition, the presence of spurious modes is observed at high frequencies (yellow circle on Fig. 13). The presence of these additional modes can be explained by the difficulty to describe the high frequency regime, especially in this p-polarization case which more demanding for the coarse mesh and the choice of edge elements.

This preliminary implementation in p-polarization needs further development which will be presented in a future work.

## V. CONCLUSION

In this paper, the so-called “resonance formalism” has been implemented into the Finite Element Method in order to perform modal analysis of dispersive and dissipative photonic structures. The method has been first validated in the simple case of a closed cavity and then

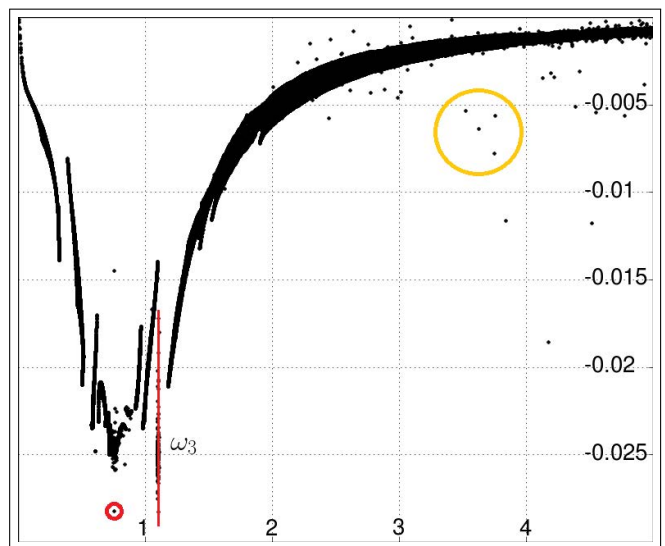


FIG. 13. Spectrum of the normalized resonances  $\omega_n a / (2\pi c)$  in the photonic crystal made of rods of Drude p-polarization. Spurious modes produced by  $\epsilon(\omega_3) = 0$  are highlighted with red color. Spurious modes at high frequency are highlighted with yellow color.

used in the case of two-dimensional crystals. The numerical results obtained in s-polarization are in excellent agreement with previous results in the literature and obtained with completely different numerical methods. As to results obtained in p-polarization, they suffer from the presence of spurious modes which, in the case of the used FEM method, can be explained by the non-fulfillment of the divergence condition when the permittivity vanishes.

For s-polarization, the numerical method presented in this paper provides an efficient tool to compute and analyze the complex spectrum of dispersive systems and non self-adjoint operators which have been rarely explored. The present results confirm that retrieving the resonances for wavevectors corresponding to the boundary of the first reduced Brillouin zone is not sufficient to catch the whole spectrum of photonic crystals. In particular, the presence of critical points and branches have been highlighted in the inside of the reduced Brillouin zone. Also, it has been shown that the phenomenon of resonances outgoing of the contour is associated to an interlacing of bands. However, no argument has been found to explain this interlacing of bands, particularly a coupling of modes could not be evidenced. In addition to this

band interlacing, cusps and loops have been highlighted in the band structure, which could have interesting effect on the group velocity.

Further developments of the present method are required to be applied on open-systems and 3D structures. Regarding open-systems, the solution is to use Perfectly Matched Layer damping the field in free space [22]. For 3D systems, a solution to avoid spurious modes while using edge elements in the FEM has to be developed.

## FUNDING INFORMATION

This work is supported by the Agence Nationale de la Recherche (project PLANISSIMO ANR-12-NANO-0003).

## ACKNOWLEDGMENT

Philippe Lalanne (CNRS, LP2N, France) is acknowledged for fruitful discussions.

- 
- [1] J. D. Jackson, *Classical electrodynamics* (Wiley, New York, NY, 1999), 3rd ed.
- [2] J.-M. Combes, B. Gralak, and A. Tip, "Spectral properties of absorptive photonic crystals," *Contemp. Math.* **339**, 1 (2002).
- [3] H. van der Lem, A. Tip, and A. Moroz, "Band structure of absorptive two-dimensional photonic crystals," *JOSA B* **20**, 1334-1341 (2003).
- [4] B.-Y. Gu, L.-M. Zhao, and Y.-C. Hsue, "Applications of the expanded basis method to study the properties of photonic crystals with frequency-dependent dielectric functions and dielectric losses," *Physics Letters A* **355**, 134-141 (2006).
- [5] G. Alagappan and A. Deinega, "Optical modes of a dispersive periodic nanostructure," *Progress In Electromagnetics Research B* **52**, 1-18 (2013).
- [6] O. Toader and S. John, "Photonic band gap enhancement in frequency-dependent dielectrics," *Physical Review E* **70**, 046605 (2004).
- [7] G. Demésey and S. John, "Solar energy trapping with modulated silicon nanowire photonic crystals," *Journal of Applied Physics* **112**, 074326 (2012).
- [8] A. H. B. Ghasemi, S. Mandegarian, H. Kebriti, and H. Latifi, "Bandgap generation and enhancement in polaritonic cylinder square-lattice photonic crystals," *Journal of Optics* **14**, 055103 (2012).
- [9] A. Raman and S. Fan, "Photonic band structure of dispersive metamaterials formulated as a hermitian eigenvalue problem," *Phys. Rev. Lett.* **104**, 087401 (2010).
- [10] A. Tip, "Canonical formalism and quantization for a class of classical fields with application to radiative atomic decay in dielectrics," *Phys. Rev. A* **56**, 5022 (1997).
- [11] A. Tip, "Linear absorptive dielectrics," *Phys. Rev. A* **57**, 4818 (1998).
- [12] D. Barchiesi and T. Grosjes, "Errata: Fitting the optical constants of gold, silver, chromium, titanium and aluminum in the visible bandwidth," *J. Nanophotonics* **8**, 089996 (2014).
- [13] A. Figotin and J. Schenker, "Hamiltonian structure for dispersive and dissipative dynamical systems," *J. Stat. Phys.* **128**, 969 (2007).
- [14] B. Gralak and A. Tip, "Macroscopic maxwells equations and negative index materials," *J. Math. Phys.* **51**, 052902 (2010).
- [15] K. S. Yee *et al.*, "Numerical solution of initial boundary value problems involving maxwell's equations in isotropic media," *IEEE Trans. Antennas Propag* **14**, 302-307 (1966).
- [16] J. E. Roman, C. Campos, E. Romero, and A. Tomas, "SLEPc users manual," *Tech. Rep. DSIC-II/24/02 - Revision 3.6*, D. Sistemes Informàtics i Computació, Universitat Politècnica de València (2015).
- [17] A. Nicolet, S. Guenneau, C. Geuzaine, and F. Zolla, "Modelling of electromagnetic waves in periodic media with finite elements," *J. Comput. Appl. Math.* **168**, 321 (2004).
- [18] P. Dular, A. Nicolet, A. Genon, and W. Legros, "A discrete sequence associated with mixed finite elements and its gauge condition for vector potentials," *Magnetics, IEEE Transactions on* **31**, 1356 (1995).
- [19] C. Geuzaine and J.-F. Remacle, "Gmsh: A 3-d finite element mesh generator with built-in pre-and post-processing facilities," *Int. J. Numer. Meth. Eng.* **79**, 1309 (2009).
- [20] P. Dular *et al.*, "A general environment for the treatment of discrete problems and its application to the finite element method," *IEEE Trans. Magn.* **34**, 3395 (1998).

- [21] B. Gralak, M. de Dood, G. Tayeb, S. Enoch, and D. Maystre, "Theoretical study of photonic band gaps in woodpile crystals," *Phys. Rev. E* **67**, 066601 (2003).
- [22] J.-P. Berenger, "A perfectly matched layer for the absorption of electromagnetic waves," *J. Comp. Phys.* **114**, 185 (1994).

## VI. APPENDIX

### A. Extension to the absorptive case of the purely dispersive auxiliary field formalism.

A material with relative permittivity described by a single Drude-Lorentz resonance is considered. With  $\omega_r = \sqrt{\omega_D^2 - \gamma_D^2/4}$  and  $\omega_{\pm} = \pm\omega_r - i\gamma_D/2$ , the expression (36) becomes

$$\begin{aligned} \epsilon(\omega) &= \epsilon_{\infty} - \frac{\omega_p^2}{\omega^2 + i\gamma_D\omega - \omega_D^2} = \epsilon_{\infty} - \frac{\omega_p^2}{(\omega - \omega_+)(\omega - \omega_-)} \\ &= \epsilon_{\infty} - \frac{\omega_p^2}{2\omega_r} \left[ \frac{1}{\omega - \omega_+} - \frac{1}{\omega - \omega_-} \right]. \end{aligned} \quad (36)$$

The corresponding dielectric susceptibility  $\chi$  can be retrieved through the inverse Fourier transform of  $\epsilon(\omega) - \epsilon_{\infty}$ :

$$\chi(t) = -\frac{1}{2\pi} \int_{\mathbb{R}} d\omega \frac{\exp(-i\omega t)\omega_p^2}{[\omega - \omega_+][\omega - \omega_-]}. \quad (37)$$

For negative time, this integral is computed by closing the loop in the upper half plane of complex frequencies  $\omega$ . Since the function under the integral in Eq. (37) has no pole in the upper half plane, the dielectric susceptibility vanishes according to the causality principle. For positive time, the integral is now computed by closing the loop in the lower half plane of frequencies  $\omega$  with negative imaginary part. The function under the integral has now two poles in the lower half plane at  $\omega_{\pm}$ . Using the Cauchy residue theorem, the dielectric susceptibility is obtained:

$$\begin{aligned} \chi(t) &= \frac{\omega_p^2}{2i\omega_r} \{ \exp[-i\omega_-t] - \exp[-i\omega_+t] \} \\ &= \frac{\omega_p^2}{\omega_r} \exp[-t\gamma_D/2] \sin[\omega_r t]. \end{aligned} \quad (38)$$

Maxwell's equations without sources in the time regime for the considered material are written:

$$\begin{aligned} \nabla \times \mathbf{E}(\mathbf{r}, t) &= -\mu_0 \frac{\partial \mathbf{H}}{\partial t}(\mathbf{r}, t) \\ \nabla \times \mathbf{H}(\mathbf{r}, t) &= \frac{\partial \mathbf{D}}{\partial t}(\mathbf{r}, t) = \frac{\partial [\epsilon_0 \epsilon_{\infty} \mathbf{E}(\mathbf{r}, t) + \mathbf{P}(\mathbf{r}, t)]}{\partial t}, \end{aligned} \quad (39)$$

where  $\mathbf{D}$  and  $\mathbf{P}$  are the displacement and polarization fields. Noticed that  $\epsilon_{\infty}$  in Eq. (39) is considered as a constant relative permittivity acting directly on the electric field, and not a part of the polarization field. This choice has been made since the expression of the polarization

requires a time convolution for a rigorous formulation of the problem. In real world this trick does not appear since the constant  $\epsilon_{\infty}$  must take the unit value. However, this additional parameter is introduced because it allows efficient fit of the real permittivity of metals [12].

The polarization field is given by

$$\mathbf{P}(\mathbf{r}, t) = \epsilon_0 \int_{-\infty}^t ds \chi(\mathbf{r}, t-s) \mathbf{E}(\mathbf{r}, s). \quad (40)$$

Using (38), the expression of the time derivative of the polarization field (also called the microscopic currents) is obtained:

$$\begin{aligned} \frac{\partial \mathbf{P}}{\partial t}(\mathbf{r}, t) &= \epsilon_0 \frac{\partial}{\partial t} \int_{-\infty}^t ds \chi(\mathbf{r}, t-s) \mathbf{E}(\mathbf{r}, s) \\ &= \epsilon_0 \chi(\mathbf{r}, 0) \mathbf{E}(\mathbf{r}, t) + \epsilon_0 \int_{-\infty}^t ds \frac{\partial \chi}{\partial t}(\mathbf{r}, t-s) \mathbf{E}(\mathbf{r}, s) \\ &= \epsilon_0 \frac{\omega_p^2}{2\omega_r} \omega_+ \int_{-\infty}^t ds \exp[-i\omega_+(t-s)] \mathbf{E}(\mathbf{r}, s) \\ &\quad - \epsilon_0 \frac{\omega_p^2}{2\omega_r} \omega_- \int_{-\infty}^t ds \exp[-i\omega_-(t-s)] \mathbf{E}(\mathbf{r}, s). \end{aligned} \quad (41)$$

Hence the two auxiliary fields defined below appear naturally

$$\mathbf{A}_L^{\pm}(\mathbf{r}, t) = \mp i \frac{\omega_p}{\sqrt{2}\omega_r} \omega_{\pm} \int_{-\infty}^t ds \exp[-i\omega_{\pm}(t-s)] \mathbf{E}(\mathbf{r}, s), \quad (42)$$

and the time derivative of the polarization field becomes

$$\frac{\partial \mathbf{P}}{\partial t}(\mathbf{r}, t) = i\epsilon_0 \frac{\omega_p}{\sqrt{2}} \mathbf{A}_L^+(\mathbf{r}, t) + i\epsilon_0 \frac{\omega_p}{\sqrt{2}} \mathbf{A}_L^-(\mathbf{r}, t). \quad (43)$$

Finally, Maxwell's equations result in the set of equations (10), denominated as the "resonance formalism".

For a Drude resonance, similar arguments lead to the definition of the auxiliary field Eq. (16) and Maxwell's equations become (17).

### B. Eigenfrequencies of closed dispersive cavities.

The expressions (28) and (29) of the dispersion law are established for the system considered in section 3, and which is made of two square domains (side length  $a$ ) of permittivity  $\epsilon_1(\omega)$  and  $\epsilon_2(\omega)$ .

#### 1. *s*-polarization.

In this case, the electric field has a single component  $E(x, y, \omega)$  along the  $z$ -axis and Dirichlet boundary conditions are imposed on the boundary of the domain. The following eigenvalue problem has to be solve:

$$\left[ \frac{\partial^2}{\partial x^2} + \frac{\partial^2}{\partial y^2} + \omega_n^2 \epsilon(\omega_n) \epsilon_0 \mu_0 \right] E_n(x, y) = 0 \quad (44)$$

Using the separation of variables, the eigenfunctions  $E_n$  are determined with the decomposition

$$E_n(x, y) = \phi_p(x)\psi_q(y). \quad (45)$$

The solution in the  $y$  direction is just

$$\psi_q(y) = \sin[q\pi y/a], \quad q \in \mathbb{N} \setminus \{0\}, \quad (46)$$

which ensures the Dirichlet boundary conditions. This solution is injected in the equation (44):

$$\frac{d^2\phi_p}{dx^2}(x) + [\omega_n^2\epsilon(\omega_n)\epsilon_0\mu_0 - q^2\pi^2/a^2] \phi_p(x) = 0. \quad (47)$$

The propagation constants are defined as

$$\beta_j(\omega_n) = \sqrt{\frac{\omega_n^2}{c^2}\epsilon_1(\omega_n) - \frac{q^2\pi^2}{a^2}}, \quad j = 1, 2, \quad (48)$$

and the equation (47) becomes

$$\begin{cases} [d^2\phi_p/dx^2](x) + \beta_1^2(\omega_n)\phi_p(x) = 0 & \text{if } x < 0 \\ [d^2\phi_p/dx^2](x) + \beta_2^2(\omega_n)\phi_p(x) = 0 & \text{if } x > 0 \end{cases}. \quad (49)$$

The general solution of these equations are

$$\begin{cases} \phi_p(x) = A_1 \cos[\beta_1(\omega_n)x] + B_1 \sin[\beta_1(\omega_n)x] & \text{if } x < 0 \\ \phi_p(x) = A_2 \cos[\beta_2(\omega_n)x] + B_2 \sin[\beta_2(\omega_n)x] & \text{if } x > 0 \end{cases} \quad (50)$$

The four unknowns are determined using the four boundary conditions:  $\phi_p(-a) = 0$ ,  $\phi_p(a) = 0$ ,  $\phi_p(0^-) = \phi_p(0^+)$

and  $[d\phi_p/dx](0^-) = [d\phi_p/dx](0^+)$ . This leads to the following set of equations

$$\begin{cases} A_1 \cos[\beta_1(\omega_n)a] = B_1 \sin[\beta_1(\omega_n)a] \\ A_2 \cos[\beta_2(\omega_n)a] = -B_2 \sin[\beta_2(\omega_n)a] \\ A_1 = A_2 \\ B_1\beta_1(\omega_n) = B_2\beta_2(\omega_n) \end{cases}. \quad (51)$$

The existence of a non vanishing solution to this set of equations provides the dispersion equation of the system:

$$\frac{\tan[\beta_1(\omega_n)a]}{\beta_1(\omega_n)} + \frac{\tan[\beta_2(\omega_n)a]}{\beta_2(\omega_n)} = 0. \quad (52)$$

## 2. $p$ -polarization.

In this case, the magnetic field has a single component  $H(x, y, \omega)$  along the  $z$ -axis and Neumann boundary conditions are imposed on the boundary of the domain.

The different steps presented in the  $s$  polarization case can be used. The first difference is the expression of the solution in the  $y$  direction

$$\psi_q(y) = \cos[q\pi y/a], \quad q \in \mathbb{N}, \quad (53)$$

which now ensures the Neumann boundary conditions. And the second difference is the boundary conditions used to solve the system (50) which are now:  $[d\phi_p/dx](-a) = 0$ ,  $[d\phi_p/dx](a) = 0$ ,  $\phi_p(0^-) = \phi_p(0^+)$  and  $\epsilon_2(\omega_n)[d\phi_p/dx](0^-) = \epsilon_1(\omega_n)[d\phi_p/dx](0^+)$ . The resulting linear set of equations is

$$\begin{cases} A_1 \sin[\beta_1(\omega_n)a] = -B_1 \cos[\beta_1(\omega_n)a] \\ A_2 \sin[\beta_2(\omega_n)a] = B_2 \cos[\beta_2(\omega_n)a] \\ A_1 = A_2 \\ B_1\beta_1(\omega_n)/\epsilon_1(\omega_n) = B_2\beta_2(\omega_n)/\epsilon_2(\omega_n) \end{cases}. \quad (54)$$

Again, the existence of a non vanishing solution to this set of equations provides the dispersion equation of the system:

$$\frac{\beta_1(\omega_n)}{\epsilon_1(\omega_n)} \tan[\beta_1(\omega_n)a] + \frac{\beta_2(\omega_n)}{\epsilon_2(\omega_n)} \tan[\beta_2(\omega_n)a] = 0. \quad (55)$$